# Convexity and Stiffness in Energy Functions for Electrostatic Simulations

Justine S. Pujos* and A. C. Maggs*

Laboratoire PCT, Gulliver CNRS-ESPCI UMR 7083, 10 rue Vauquelin, 75231 Paris Cedex 05, France

ABSTRACT: We study the properties of convex functionals which have been proposed for the simulation of charged molecular systems within the Poisson−Boltzmann approximation. We consider the extent to which the functionals reproduce the true fluctuations of electrolytes and thus the one-loop correction to mean field theory—including the Debye−Hückel correction to the free energy of ionic solutions. We also compare the functionals for use in numerical optimization of a mean field model of a charged polymer and show that different functionals have very different stiffnesses leading to substantial differences in accuracy and speed.
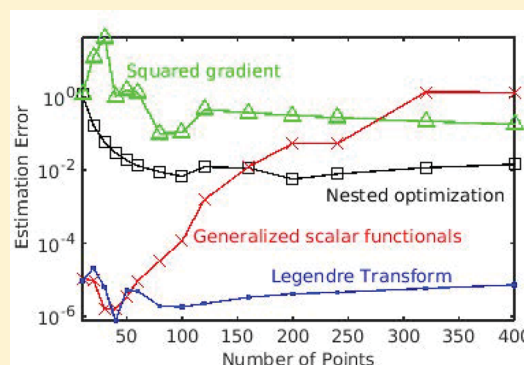
■ INTRODUCTION

The sign of electrostatic free energy functionals has long interested and puzzled the community of molecular simulators: A recent paper states, *"The fact that the functional cannot be identified with the electrostatic energy away from the minimum a priori precludes its use in a dynamical "on the fly" optimization..."*[1] Similar statements as to the nature of the free energy in Poisson−Boltzmann functionals can be found in other papers.[2,3]

Implicitly, most formulations of electrostatic free energies work [an exception is ref 4] with the electric field and the potential and are associated with the natural potential energy

$$U_E = -\int \frac{\varepsilon \mathbf{E}^2}{2} d\mathbf{r} \qquad (1)$$

This energy seems to be concave and unbounded below, whereas when thermodynamic potentials are written in terms of the electric displacement field $\mathbf{D}$, we find

$$U_D = +\int \frac{\mathbf{D}^2}{2\varepsilon} d\mathbf{r} \qquad (2)$$

which is convex. As emphasized in a classic text,[5] the two formulations are identical in content and simply linked by a Legendre transform. The importance of the correct ensemble in the understanding of electrodynamics and stability of media was particularly emphasized in reviews of Kirzhnits and collaborators.[6,7] Inspired in particular by this view, we proposed a free energy functional for the Poisson−Boltzmann equation which is a true minimizer,[8,9] rather than a stationary principle. Our hope is that when implemented in practical codes[10] these locally formulated convex forms give more stable and simpler algorithms. Using a convex free energy, it is possible to implement an implicit solvent code which fully includes the Poisson−Boltzmann free energy in which "on the fly"

optimization can then be performed using the Car−Parrinello method.[11] In this case, the electrodynamic field can evolve in parallel to degrees of freedom in the molecule.[12]

Our work takes the displacement field $\mathbf{D}$ as the fundamental thermodynamic field, rather than ϕ or $\mathbf{E}$. Other recent work[13−15] takes a different approach to the problem. By a series of transformations to the original variational formulations of the Poisson−Boltzmann functional (expressed as a function of the electrostatic potential, ϕ), the authors have found new families of functionals which are scalar, convex, and local.

While all these functionals are strictly equivalent at their stationary point, when simulating at finite temperatures differences can occur: The Car−Parrinello method thermostats the supplementary variables to zero temperature; in this way, we only see the true minimum of the energy functional. However, in many applications, we might wish to run simulations with *all variables thermostated to the same, ambient temperature*. For electrostatic functionals in dielectric media, this samples fluctuations which are equivalent to the so-called thermal Casimir interaction,[16−18] which is just the zero frequency contribution to the free energy in Lifshitz theory. There thus arises the question: what happens to the free energies when a convex Poisson−Boltzmann functional is used in a finite temperature simulation? One might hope that the functionals also reproduce the correct one-loop corrections to the free energy, which in the case of an electrolyte has an anomalous scaling in $\rho^{3/2}$ where ρ is the salt concentration.

To answer this question, we will study the spectra of several free energy functionals expanded to quadratic order. The spectra are also crucial in understanding the convergence properties and dynamics of simulation algorithms. Accurate

(non-implicit) integration in molecular dynamics requires a time step which is short compared with all dynamic processes under consideration. Algorithms which generate time scales which are very different for different modes are said to be *stiff* and lead to reduced efficiency. Stiffness can also have other, unwanted consequences in optimization algorithms—such as poor convergence properties. We explore this question in the last part of the paper where we study a model of free energy minimization in the context of a confined polyelectrolyte.

We start with a reminder of Poisson−Boltzmann theory and the corrections to it coming from Gaussian fluctuations at the one-loop level. We then show that the same one-loop free energy is found in a complementary dual (and convex) formulation of the free energy which can be used within a full molecular dynamics or Monte Carlo simulation. We then move on to considerations of coarse grained models and test various discretizations of electrostatic energies for their accuracy and ease of use within minimizing principles.

POISSON−BOLTZMANN THEORY AND ITS ONE-LOOP CORRECTION

In our presentation, we will consider the case of a symmetric electrolyte; however the identities that we derive are independent of the exact microscopic model used. The use of a definite physical example leads to considerable simplification of notation.

The mean-field Poisson−Boltzmann functional for a symmetric electrolyte is

$$F_\phi = \int \left(-\frac{\varepsilon(\nabla\phi)^2}{2} - 2k_\mathrm{B}T\lambda \cosh \beta e\phi + \rho_e\phi \right) \mathrm{d}\mathbf{r} \quad (3)$$

where $k_\mathrm{B}T = \beta^{-1}$ is the thermal energy, e the ion charge, ϕ the electrostatic potential, and λ a fugacity. At the stationary point of this "free energy," we find

$$\mathrm{div}\ \varepsilon\ \mathrm{grad}\ \phi - 2\lambda e\ \sinh(\beta e\phi) + \rho_e = 0 \quad (4)$$

which is indeed the classic equation for the potential in the Poisson−Boltzmann formalism. Linearizing this equation allows us to define the inverse Debye length from $\kappa^2 = 2\lambda\beta e^2/\varepsilon$. At low concentrations, λ can be identified with the salt concentration. Since this thermodynamic potential is naturally expressed in terms of the thermodynamic fields ϕ or $\mathbf{E}$, it is concave as noted for eq 1. Any attempt to use such a form in a Car−Parrinello simulation will lead to numerical instabilities.

Much recent work has used field theory techniques to extend this functional to include fluctuations. In particular, one can sum the fluctuations to the *one-loop* level,[19,20] which gives as a correction to this free energy the functional determinant

$$F_\mathrm{loop} = \frac{k_\mathrm{B}T}{2}\log|- \mathrm{div}\ \varepsilon(r)\mathrm{grad}\phi + 2\lambda\beta e^2 \cosh(\beta e\phi)| \quad (5)$$

This expression is often interpreted with a subtraction scheme—one compares with the free energy of an empty box, where $\lambda = 0$. Even with this subtraction, the expression is formally divergent. However, on introducing a microscopic cut-off,[21] the loop free-energy gives both the Born self-energy of solvation

$$E_\mathrm{Born} = \frac{e^2}{8\pi\varepsilon a} \quad (6)$$

as well as the anomalous Debye−Hückel free energy

$$\frac{F_\mathrm{DH}}{V} = -\frac{k_\mathrm{B}T\kappa^3}{12\pi} \quad (7)$$

as is shown in Appendix II.

PROPERTIES OF THE LEGENDRE TRANSFORM

As noted above, many of the standard concave expressions for electrostatic free energies can be rendered convex by Legendre transform.[8] Several conventions exist in the literature.[22] In particular, we define the transform of a convex function $c(x)$ as

$$g(s) = \sup_x(sx - c(x)) \quad (8)$$

We will also use the notation $g(s) = \mathcal{L}[c](s)$. The transformation is an *involution*; that is, the double transform of a convex function is the identity.

For this paper, we will be interested in the second order expansion of free energies about an equilibrium point. For this, we will use an important identity linking the second derivatives of the functions g and c.

$$\frac{d^2c}{dx^2}\frac{d^2g}{ds^2} = 1 \quad (9)$$

valid at the corresponding pair of variables (x, s). We also note that the Legendre transform of a scaled function, $\alpha c(\gamma x)$, is given by $\alpha g(s/(\alpha\gamma))$.

DUAL FORMULATIONS OF THE POISSON−BOLTZMANN EQUATION

In previous work,[8,9] we have detailed how to pass from the Poisson−Boltzmann free energy expressed in terms of the electrostatic potential, ϕ, to a dual formulation expressed in terms of the electric displacement $\mathbf{D}$. In particular, we found

$$F_\mathrm{dual} = F_\mathrm{field} + F_\mathrm{ions} \quad (10)$$

where

$$F_\mathrm{field} = \mathcal{L}[\varepsilon\mathbf{E}^2/2] = \frac{\mathbf{D}^2}{2\varepsilon} \quad (11)$$

with $\mathbf{E} = -\mathrm{grad}\ \phi$ and

$$F_\mathrm{ions} = \mathcal{L}[2\lambda k_\mathrm{B}T \cosh(e\beta\phi)](\mathrm{div}\ \mathbf{D} - \rho_e) \quad (12)$$

The transform of the hyperbolic cosine is easily found

$$g(s) = \mathcal{L}[2 \cosh](s) = s \sinh^{-1}(s/2) - \sqrt{4 + s^2} \quad (13)$$

thus

$$F_\mathrm{dual} = \int \left(\frac{\mathbf{D}^2}{2\varepsilon} + k_\mathrm{B}T\lambda g((\mathrm{div}\ \mathbf{D} - \rho_e)/e\lambda) \right) \mathrm{d}\mathbf{r} \quad (14)$$

This form as a sum of two Legendre transforms will turn out to be very important for a number of determinant identities that we derive below. We will need also the expansion of $g(s) = -2 + s^2/4 - s^4/192 + ...$

This transformation gives a convex free energy which can be used in a Monte Carlo or molecular dynamics simulation. It has been constructed so that the minimum of eq 14 is identical to the maximum of eq 3. The potential and dual formulations are linked via the equation

$$\mathrm{div}\ \mathbf{D} - \rho_e = -2\lambda e\ \sinh(\beta e\phi) \quad (15)$$

which can be understood as showing that the ionic charge concentration in the Poisson−Boltzmann equation is $-2\lambda e \sinh \beta e\phi$.

Parameterization and Scalarizing. It is clear that the use of a vector functional rather than the usual scalar form has increased the number of variables that need to be simulated or optimized.[14,15] We show here that given a functional eq 14 of a vector field, we can find a related functional of a scalar field.

When we consider the stationary point of the energy eq 14, we find that

$$\frac{\mathbf{D}}{\varepsilon} - \frac{k_B T}{e}\text{grad } g' = 0 \tag{16}$$

We then identify the function $k_B T g'/e = -\phi$ at the stationary point. We see that we can make such a substitution even away from the minimum to find a more restrictive functional which is to be optimized over a smaller subspace:

$$F_{\text{dual},\phi} = \int \left(\varepsilon\frac{(\nabla\phi)^2}{2} + k_B T\lambda g((\text{div }\varepsilon\text{ grad }\phi + \rho_e)/e\lambda) \right) d\mathbf{r} \tag{17}$$

Since the space is more restrictive, the minimum of this functional is clearly greater than or equal to the functional expressed in terms of $\mathbf{D}$; however, the absolute minimum is compatible with the parametrization, implying that this functional has the correct minimum free energy. Indeed, we can go further and take linear combinations

$$F_{\text{comb}} = (m + 1)F_{\text{dual},\phi} + mF_\phi \tag{18}$$

for $m \geq 0$, which all have the same, correct minimum.

Determinant Identities. In this section, we present some matrix identities which link the functional determinants of operators with their dual equivalent. These identities are particularly interesting because they link operators (at least when discretized) of dimensions $N \times N$, which are expressed in terms of the potential, to operators of dimensions $3N \times 3N$ for the electric displacement.

The identities are easiest to derive from a discretized form of the free energy. We will work with the discrete divergence operator ∂_{rl} which acts on the link variable D_l. When discretizing to a simple cubic lattice, there are $3N$ variables D_l and N values of the divergence which we associate with the lattice points. We discretize the nonlinear contribution to the free energy eq 14 as follows:

$$F_{\text{ions}} = \sum_r g\left(\sum_l \partial_{rl}D_l - \rho_e\right) \tag{19}$$

Take a second derivative with respect to the link variables D_p and D_q to find the matrix

$$\Delta_{pq} = \sum_r \partial_{rp}\partial_{rq}g''\left(\sum_l \partial_{rl}D_l - \rho_e\right) \tag{20}$$

where g'' is the second derivative of g, evaluated at r. Create a matrix with g'' on the diagonal, then eq 20 is a conventional matrix product:

$$\Delta_{pq} = \sum_{rr'} \partial_{pr}^T(g''_r\delta_{rr'})\partial_{r'q} \tag{21}$$

We identify $(-\partial_{pr}^T)$ with the gradient operator since div and $(-\text{grad})$ are mutually adjoint.

We similarly discretize the gradient contribution to the free energy eq 3

$$\frac{1}{2}\sum_{rr',l}\varepsilon_l(\partial_{lr}^T\phi_r)(\partial_{lr'}^T\phi_{r'}) \tag{22}$$

and take the second derivative with respect to ϕ_r to find the matrix

$$\tilde{\Delta}_{rr'} = \sum_l \varepsilon_l\partial_{lr}^T\partial_{lr'}^T \tag{23}$$

When we turn ε_l into a diagonal matrix, we find the matrix product

$$\tilde{\Delta}_{rr'} = \sum_{ll'} \partial_{r'l}(\varepsilon_l\delta_{ll'})\partial_{l'r}^T \tag{24}$$

which is the discrete version of the operator $(-\text{div }\varepsilon\text{ grad})$.

We now consider the relation between the one-loop free energy, eq 5, and its naive equivalent within the dual formulation found by taking the second functional derivative of eq 14, which we write as the discretized form:

$$F_{\text{dual,loop}} = \frac{k_B T}{2}\left|\frac{\delta_{ll'}}{\varepsilon_l} + \partial^T g''\partial\right| \tag{25}$$

We will show that, modulo some trivial local contributions to the free energy, the expression eq 25 contains the same physics as eq 5, which we write as

$$F_{\text{loop}} = \frac{k_B T}{2}|\partial\varepsilon\partial^T + c''| \tag{26}$$

where c'' is the second derivative of the entropic contribution to the free energy. In the case of the symmetric electrolyte, $c = 2k_B T\lambda \cosh(e\beta\phi)$.

To link these two determinants, we will make use of the singular value decomposition theorem, which states that a *rectangular matrix*, $\mathbf{A}$, of dimensions $m \times n$ can be expressed as a product

$$\mathbf{A} = \mathbf{U\Sigma V}^* \tag{27}$$

where U is an unitary matrix of dimensions $m \times m$ such that $UU^* = U^*U = 1$; V is also unitary of dimensions $n \times n$, and Σ is diagonal rectangular with non-negative elements on the diagonal.

We consider the determinant for a rectangular matrix $\mathbf{A}$:

$$|\mathbf{AA}^T + 1| \tag{28}$$

With the help of the singular value decomposition, we can write

$$|1 + \mathbf{AA}^T| = |1 + \mathbf{U\Sigma\Sigma}^T\mathbf{U}^*| = |1 + \mathbf{\Sigma\Sigma}^T| \tag{29}$$

$$= |1 + \mathbf{\Sigma}^T\mathbf{\Sigma}| = |1 + \mathbf{A}^T\mathbf{A}| \tag{30}$$

The identity is between two matrices of different dimensions: $m \times m$ and $n \times n$. We apply this theorem to

$$\mathbf{A} = \frac{1}{\sqrt{c''}}\partial\sqrt{\varepsilon} \tag{31}$$

and find

$$\left|\frac{1}{\sqrt{c''}}\partial\varepsilon\partial^T\frac{1}{\sqrt{c''}} + 1\right| = \left|\sqrt{\varepsilon}\partial^T\frac{1}{c''}\partial\sqrt{\varepsilon} + 1\right| \tag{32}$$

We can pull the diagonal matrices c'' and ε out of the main determinants to find

$$|\partial\varepsilon\partial^T + c''| = |c''||\varepsilon|\left|\partial^T\frac{1}{c''}\partial + \frac{1}{\varepsilon}\right| \tag{33}$$

We now make use of the relation between the curvatures of a function and its Legendre transform eq 9: $g'' = 1/c''$, so that

$$|\partial \varepsilon \partial^T + c''| = |c''| |\varepsilon| \left|\partial^T g'' \partial + \frac{1}{\varepsilon}\right| \tag{34}$$

which is our required identity. The result is rather remarkable. The dual energy eq 14 was derived purely by considering stationary properties of the free energy. *However*, if we use this in a simulation at finite temperature, *we generate automatically the correct one loop free energy*, modulo a trivial shift in the zero. Of course, we do not have any guarantee that any higher order contributions are correct—in particular in the strong coupling limit[23−25] the addition of terms valid in a weak coupling expansion may not help in correctly describing the physics. We can also write the dual contribution to the free energy as

$$F_{\text{dual,loop}} = \frac{k_{\text{B}}T}{2} \log\left| - \text{grad } g'' \text{div} + \frac{1}{\varepsilon}\right| \tag{35}$$

For the specific case of a symmetric electrolyte, $d^2g/ds^2 = (1/(4 + s^2)^{1/2})$.

As noted in a recent paper, the one-loop corrected Poisson−Boltzmann equation contains many interesting physical effects including image charges in the case of dielectric continuities.[21,26] Thus, having a form of the Poisson−Boltzmann that can be simulated and that includes such terms could be particularly interesting in applications near surfaces.

■ GENERAL SCALAR FUNCTIONALS

Entirely different approaches to convexification have also been proposed in a recent series of papers.[13−15] In particular, it was shown that it is possible to develop a local, convex functional which is expressed in terms of the scalar potential, rather than the vector field **D**. The authors give several expressions but in particular find a local minimizing principle with the functional

$$F_{sc} = \int \left[\frac{\varepsilon(\nabla\phi)^2}{2} - 2k_{\text{B}}T\lambda \cosh(\beta e\phi) + 2\lambda e\phi \sinh(\beta e\phi) \right. \tag{36}$$

$$+ \frac{k_{\text{B}}T}{e} \sinh^{-1}((\text{div } \varepsilon \text{ grad } \phi + \rho_e)/2e\lambda)$$

$$\left. \times (\text{div } \varepsilon \text{ grad } \phi + \rho_e - 2e\lambda \sinh(\beta e\phi)) \right] d\mathbf{r} \tag{37}$$

When expanded to second order in ϕ, this gives

$$F_{sc} = \text{const} + \int \left[\frac{3\varepsilon(\nabla\phi)^2}{2} + \lambda\beta e^2\phi^2 \right.$$

$$\left. + \frac{(\text{div } \varepsilon \text{ grad } \phi + \rho_e)^2}{2e^2\beta\lambda} - \rho_e\phi \right] d\mathbf{r} \tag{38}$$

At least to second order, this looks like a linear combination of eq 17 and eq 3. Far from any sources in a background and with uniform dielectric properties, we can rewrite eq 38 in Fourier space:

$$F = \sum_q \left(\frac{3\varepsilon q^2}{2} + \lambda\beta e^2 + \frac{\varepsilon^2 q^4}{2\lambda e^2\beta} \right) |\phi_q|^2 \tag{39}$$

The question that arises at this moment is whether such an expression also gives rise to the correct one-loop potential. From the dispersion relation, we deduce that the fluctuation potential can be written in the form

$$F_{\text{fluc}} = \frac{k_{\text{B}}T}{2} \sum_q \log(1 + 3(q/\kappa)^2 + (q/\kappa)^4) \tag{40}$$

which corresponds to eq 54 in Debye−Hückel theory. As can be expected, this gives rise to a divergent integral in three dimensions. However, it is not clear how to separate this expression into a Born energy with a Debye−Hückel fluctuation potential of the form given in Appendix II, eq 58. We must regularize by subtracting off $\log(q^4)$, but this still leaves a Born-like energy which has a radius which is itself a function of the Debye length. Our conclusion is that the scalar functionals are indeed correct for the ground state but do not correspond to the correct excitation spectrum of the true physical system. These functionals can be used in a Car−Parrinello scheme where they are thermostated to zero temperature to avoid fluctuations.

■ SPECTRUM AND STIFFNESS

In a uniform dielectric background far from charges, the determinant eq 5 can be diagonalized using a Fourier decomposition. The eigenvalues of the operator in eq 5 are then

$$\omega_q = \varepsilon(q^2 + \kappa^2) \tag{41}$$

We now consider the spectrum in the dual picture by expanding the free energy eq 14 to quadratic order, to find the vector equivalent of the Debye−Hückel theory.

$$F_{\text{vec}} = \text{const} + \int \left[\frac{\mathbf{D}^2}{2\varepsilon} + k_{\text{B}}T \frac{(\text{div } \mathbf{D} - \rho_e)^2}{4\lambda e^2} \right] d\mathbf{r} \tag{42}$$

The spectrum for quadratic fluctuations decomposes into a longitudinal and transverse part.

$$\omega_l = \left(\frac{1}{\varepsilon} + \frac{k_{\text{B}}Tq^2}{2\lambda e^2} \right) = \omega_0(q^2 + \kappa^2)$$

$$\omega_t = \frac{1}{\varepsilon} \tag{43}$$

We note that the functional forms of eq 41 and eq 43 are the same, which explains, at least partly, the identity between the free energies at the one-loop level.

Consider now discretizing to a grid of step h, finer than the Debye length. There is a gap in the spectrum eq 43 and the ratio of the stiffest to the softest modes scales as

$$S \sim (1/\kappa h)^2 \tag{44}$$

It is clear that this ratio can become large when using a very fine grid, in which case the system of equations describing the electrolyte can become stiff. When integrating a system with a second order algorithm in time (such as molecular dynamics), the number of time steps required to sample all modes in the system scales as $\sqrt{S}$. In a Monte Carlo simulation, we can expect that the equilibration of the electrolyte takes $O(S)$ sweeps. Stiffness slows the convergence of both molecular dynamics and Monte Carlo algorithms.

If we make a similar calculation for energy functionals such as eq 39, we find that the equations are stiffer. The spectrum can be written in the form

$$\omega = \omega_0(1 + 3(q/\kappa)^2 + (q/\kappa)^4) \tag{45}$$

which implies that on a fine grid $S \sim (1/\kappa h)^4$. For eq 17, the stiffness is given by $S \sim L/\kappa^2 h^4$ where L is the system size. The presence of higher derivatives in a functional can imply a slower algorithm, even though fewer degrees of freedom must be integrated.

We now move on to the second major topic of this paper, which is the performance of optimization algorithms that look for minima in a free energy.

■ SEARCHING FOR SADDLE POINTS

We start by noting that the minimization of a convex function is generally easy. Many algorithms can be proved to converge quickly to the correct point. As an example for general quadratic minima, the conjugate gradient method for N variables converges in N iterations. If the object being minimized is a local free energy each evaluation of the energy is itself of complexity $O(N)$. Thus, we expect that the solution time for a model discretized to N lattice points should scale as $O(N^2)$. We note that this may not be the optimal method of solution—sophisticated solvers of the Poisson–Boltzmann equation such as Aquasol are rather based on multigrid methods.[27,28]

When searching for saddle points, no such simple results can be found. Consider for instance a simple alternating scheme applied to two variables x and y with the energy

$$ f = -x^2/2 + y^2/2 + \alpha x y $$

For all α, the saddle point remains at the origin.

A simple algorithm is to alternate the two variables and optimize at each step, giving the maps:

$$ x \to \alpha y \qquad y \to y \tag{46} $$

$$ y \to -\alpha x \qquad x \to x \tag{47} $$

A cycle of updates gives the product

$$ \begin{pmatrix} x' \\ y' \end{pmatrix} = \begin{pmatrix} 0 & \alpha \\ 0 & -\alpha^2 \end{pmatrix} \begin{pmatrix} x \\ y \end{pmatrix} $$

This matrix has eigenvalues 0, α^2. We converge to the origin only when $\alpha^2 < 1$. We learn that mixed optimization over coupled convex-concave spaces can fail when the coupling between variables becomes too strong in a way which is impossible for simple convex optimization.

Such mixed saddle point optimization problems occur very often in electrostatic problems which are formulated in terms of the electrostatic potential coupled to some other, physical degree of freedom. In the field of molecular simulation, we could consider the configuration of a macromolecule described by atomistic potentials. As a more definite example, we will consider a model of a charged polyelectrolyte, in which a long polymer is described using an auxiliary field Ψ, where Ψ^2 describes the local monomer concentration.[29,30] We now consider a number of optimization techniques applied to such a system. The techniques that we try are direct nested optimization between the polymer and electrostatic potential, building a positive functional from squared derivatives, Legendre transform of the electrostatic free energy, and use of generalized scalar functionals for the electrostatics.

We evaluate the methods as a function of the discretization looking for methods that are rapid and converge easily without extra derivative information being given by the user.

A Model for Mixed Optimization in Electrostatics. We work with a model developed to study spontaneous assembly of single-stranded RNA viruses.[31,32] The genetic material of the virus is modeled by a single polyelectrolyte chain, which must insert itself into a charged capsid. The system is supplemented by a symmetric electrolytic solution. The free energy density describing the interaction between the polymer, capsid, and electrolyte is

$$ F(\phi, \Psi) = \int \left[-\frac{\varepsilon}{2} (\nabla \phi)^2 + \phi(\sigma - pe\Psi^2) \right. $$
$$ \left. - 2\lambda k_B T \cosh(\beta e \phi) + k_B T \left\{ \frac{a^2}{6}(\nabla\Psi)^2 + \frac{v}{2}\Psi^4 \right\} \right] d\mathbf{r} \tag{48} $$

The third line of this expression corresponds to the non-electrostatic interactions of the polyelectrolyte. σ is the fixed charge of the capsid, p the charge on a monomer of the polyelectrolyte, a the monomer size, and v the excluded volume of the polyelectrolyte chain. This free energy is concave with respect to ϕ and convex with respect to Ψ. These two fields interact through the coupling $pe\Psi^2\phi$. In our studies, we only consider systems with spherical symmetry, discretizing to N points, see Appendix I.

Nested Optimization. The stationary point of the functional F in eq 48 corresponds to the maximum over ϕ and the minimum over Ψ. The most direct way to find such a point is to search independently for the two extrema: one optimizes iteratively the configuration while solving the electrostatic problem at each calculation of the iterative method. The outside loop of optimization calls upon the interior one until the saddle point is reached (see Algorithm 1, Chart 1). We call this method nested optimization. It is the

Chart 1. Nested Optimization Program

```
input
    φ ← φ₀
    Ψ ← Ψ₀
    over Ψ
        over φ for Ψ_fixed ← Ψ
            minimize −F(φ, Ψ_fixed) over φ
            return φ_opt, F(φ_opt, Ψ_fixed)
        φ ← φ_opt

        φ_fixed ← φ
        minimize F(φ_fixed, Ψ) over Ψ
        return Ψ_opt, f(φ_opt, Ψ_opt)
        Ψ ← Ψ_opt

    output Ψ_OPT, φ_OPT, F(φ_OPT, Ψ_OPT)
```

kind of algorithm which is easy to implement if one has a pre-existing Poisson–Boltzmann solver which one wishes to use to study the relaxation of a biomolecular system without reformulating the energy functionals.

It is to be noted that this method differs from an iterative scheme where both search loops are on the same level but included in a general loop. The schematic view of these two programs given in Figure 1 shows these differences. The classical iterative method was implemented and tested, but no convergence could be reached. We thus focus on the nested optimization method.
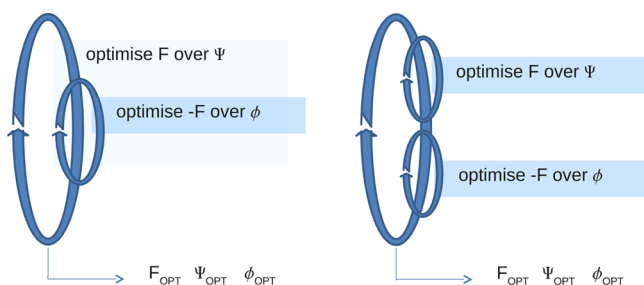
Figure 1. Schematic view of two iterative algorithms. On the left-hand side, the nested optimization method studied in this paper optimizes the free energy functional over one field for each optimization step taken for the other field. On the right-hand side, the other iterative method puts both optimization loops on the same level in a third encompassing loop.

Squared Gradient. An alternative to the nested optimization discussed above is the use of a new functional based on the gradient of the free energy.[33] At the saddle point, we have

$$\left(\frac{\delta F}{\delta \phi}\right)_{\phi_{SP}, \Psi_{SP}} = \left(\frac{\delta F}{\delta \Psi}\right)_{\phi_{SP}, \Psi_{SP}} = 0 \tag{49}$$

We can build a new functional which is always positive and vanishes at the stationary point:

$$F_{deriv}(\phi, \Psi) = \int\left[\left(\frac{\delta F}{\delta \Psi}\right)^2 + \left(\frac{\delta F}{\delta \phi}\right)^2\right] d\mathbf{r} \tag{50}$$

The minimum of this functional yields the fields at equilibrium. The advantage of this formulation is that all fields can be treated equally by the minimization process which can be managed as a single global optimization.

Generalized Scalar Functionals. The next algorithm that we test is based on eq 37. We denote $\xi(\phi, \Psi) = ((\varepsilon \nabla^2 \phi + \sigma - pe\Psi^2)/e\lambda)$ and work with the free energy

$$F_I(\phi, \Psi) = \int\left[k_B T\left\{\frac{a^2}{6}(\nabla\Psi)^2 + \frac{v}{2}\Psi^4\right\} + \frac{\varepsilon}{2}(\nabla\phi)^2 \right.$$
$$+ 2\lambda k_B T\{-\cosh(\beta e\phi) + \beta e\phi \sinh(\beta e\phi)$$
$$- \sinh^{-1}(\xi/2)\sinh(\beta e\phi)$$
$$\left. + (\xi/2)\sinh^{-1}(\xi/2)\}\right] d\mathbf{r}$$

The global minimum is found with a single optimization loop.

Legendre Transform. The Legendre transform of the electrostatic degrees of freedom is still possible in the presence of the extra polymer field. We find the locally defined free energy:

$$F_L(\mathbf{D}, \Psi) = \int\left[k_B T\left\{\frac{a^2}{6}(\nabla\Psi)^2 + \frac{v}{2}\Psi^4\right\} + \frac{\mathbf{D}^2}{2\varepsilon} \right.$$
$$\left. + k_B T\lambda g(\xi)\right] d\mathbf{r}$$

with $\xi = ((\sigma - pe\Psi^2 - \text{div } \mathbf{D})/e\lambda)$. The minimum over both Ψ and $\mathbf{D}$ is found with a single optimization loop.

■ NUMERICAL RESULTS

The four functionals were programmed in *Matlab*. We use the function *fminunc* to search for the minimum for each case. This function uses a quasi-Newton algorithm[34] and in particular the Broyden−Fletche−Goldfarb−Shanno update. The idea is to use a good, black-box minimizer to study how each formulation converges in time and accuracy as the number of discretization points increases. The ideal is a formulation that converges to high accuracy without the need for detailed tuning of the algorithm for each application. We choose to stop iteration when the functional is converged to within an estimated fraction of 10^{-12}.

Three quantities are considered to study the performance of each method: the convergence of F when the number of points increases; the derivative of the functional with respect to each field, we use the L_1-norm to test the validity of the simulation; and the simulation time as a function of N.

Variables are initialized to $\Psi = 1$ for the polyelectrolyte field and $\phi = -1$ for the potential. The system size is 24 nm, where the charge of the capsid is $\sigma = 0.4e$ at $R = 12$ nm. The bulk concentration of monovalent ions is $\lambda = 10$ mmol L^{-1} and the water relative permittivity is $\varepsilon_R = 80$. This corresponds to a Debye length of 3 nm. The parameters of the polyelectrolyte are set to $a = 0.5$ nm, $v = 0.05$ nm^3, and $p = 1$. The evolution of the free energies as a function of N is depicted in Figure 2; Figure 3 shows the derivatives on stopping.
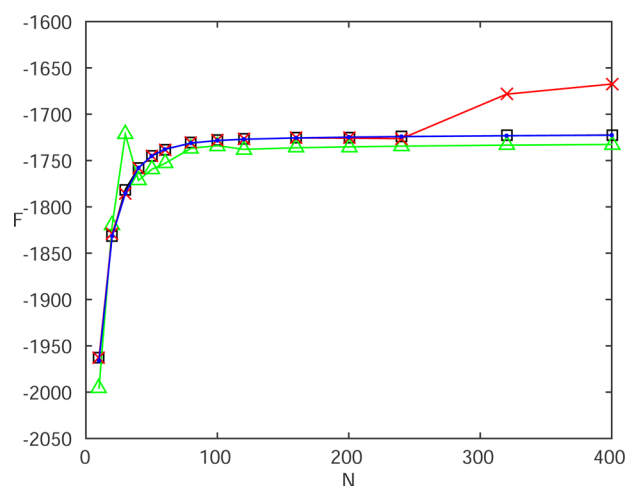

Figure 2. Convergence of free energy as a function of the number of points in the discretization. Blue dots (●): Legendre transform. Green triangles: (△) squared gradient. Black squares: (□) nested loops. Red crosses (×): generalized scalar functionals. Simple minimizer without external derivative information.

We work with values of N up to 400, which gives values of $(1/\kappa h)$, eq 44, up to 50. The discretizations are thus rather stiff. The most robust method appears to be that based on the Legendre transform. Indeed, it is the method that converges and gives the smallest error when the number of points is large, Figures 2 and 3. We note that the squared gradient method gives poor results with even small N, and the generalized scalar functional shows poor convergence for large N.

The simulation time of each method is shown in Figure 4 as a function of discretization; we use a recent intel-based desktop computer. As expected, the minimization time scales quadratically with the number of variables in the discretization. We tried other, random, initializations and found that in all cases the
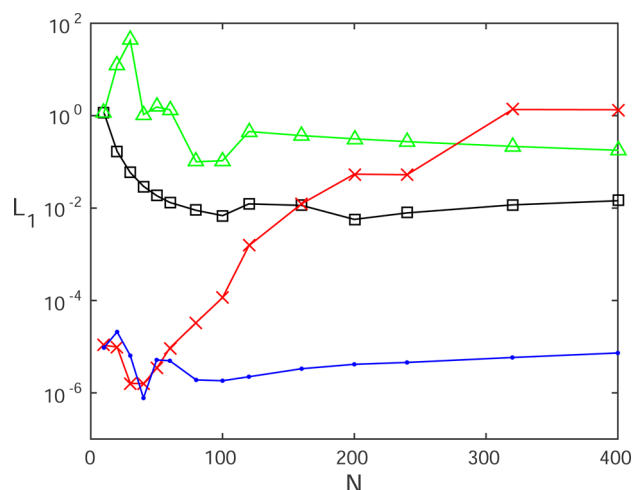
Figure 3. Derivatives of the free energy for the virus model for different discretizations and methods on exit from the optimization loop. Color code as Figure 2.
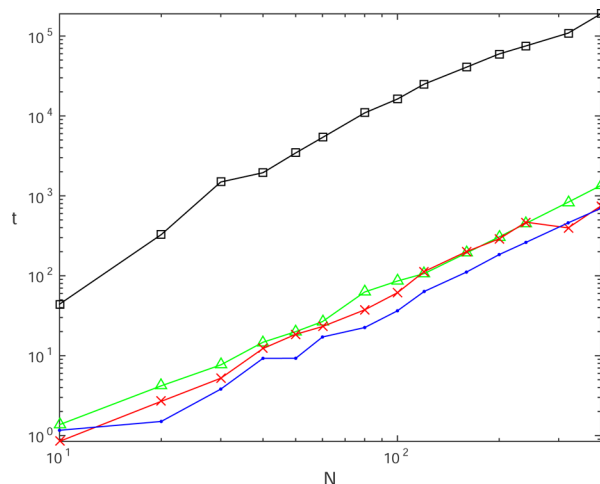
Figure 4. Total simulation time in seconds as a function of the number of points in the discretization of the free energy. All algorithms display a quadratic growth in time with N. The algorithm based on the double loop is much slower than the three other methods. Color code as Figure 2.

method based on the Legendre transform gives the most stable results, together with a time of calculation which is as good as the other tested algorithms.

■ STIFFNESS AND ALGORITHMS

From our numerical experiments we see that naive optimization of an expression with a saddle point leads to slow convergence. It is more surprising that some algorithms that can use convex optimization also give poor numerical results. One possible explanation for the differences observed between the three convex methods is that the algorithms have very different stiffnesses when the number of discretization points increases. As noted above, an algorithm based on the Legendre transform has a stiffness which increases as N^2, whereas both the squared gradient and generalized scalar functionals become much stiffer with scaling in N^4. This renders numerical codes much more susceptible to numerical round-off errors and also requires more careful stopping criteria. However, as stated above, our philosophy is that we are looking for free energies that are

stable and easy to use without large amounts of algorithmic tuning from the user.

More sophisticated black-box algorithms are also available. In particular, if we are willing to calculate and program a routine which estimates the first derivative of the free energy with respect to each variable [as is required too in molecular dynamics; these derivatives are already calculated for the square gradient method], we can find better results. In particular we use another algorithm implemented in Matlab, the *trust-region algorithm*.[35] It avoids over-large steps thanks to the limit imposed by the definition of a trust region, yet it maintains strong convergence properties. The L1-norm of the derivatives (Figure 5) and time used (Figure 6) are compared with the
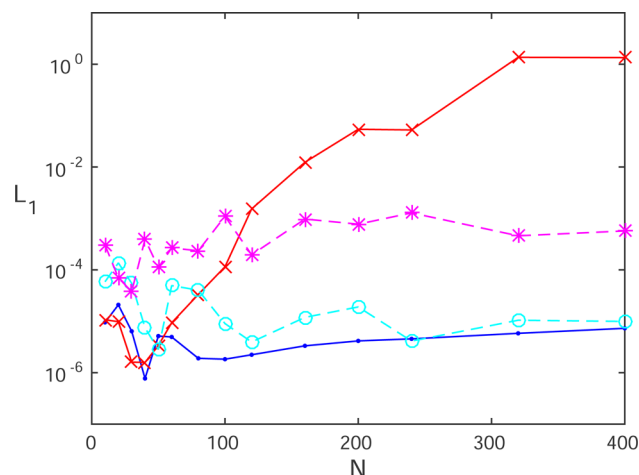
Figure 5. Derivatives of the free energy for the virus model for different discretizations and algorithms on exit from the optimization loop. Blue dots (●): Legendre transform, quasi-Newton. Cyan circles (○): Legendre transform, trust region. Red cross (✕): scalar functional, quasi-Newton. Magenta stars (∗): scalar functional, trust-region.

results obtained with the quasi-Newton algorithm. The change of algorithm allows one either to significantly reduce the computational time (Legendre transform method, blue and cyan points), or to better converge (generalized scalar functionals, red and magenta points; with the trust-region
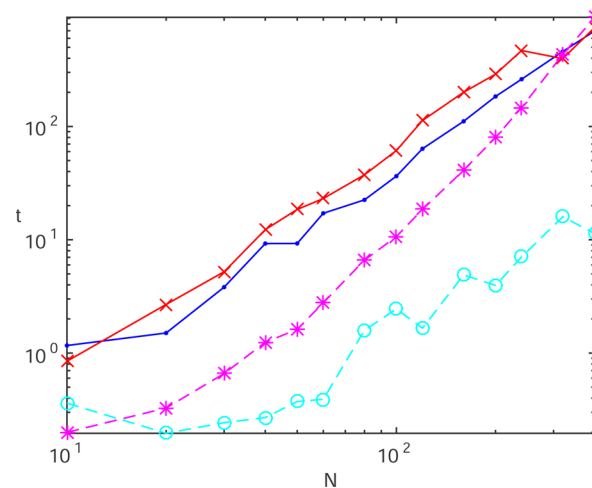
Figure 6. Computational time in seconds for different methods. Color code as for Figure 5.

algorithm, the lack of convergence of the free energy disappears). Thus, using the more sophisticated algorithm with derivative information renders the optimization more reliable or more efficient.

■ CONCLUSION

We have studied the quadratic fluctuations around equilibrium for several expressions for the free energy of charged media. These fluctuations are closely related to dispersion energies and the Debye–Hückel contribution to the free energy of electrolytes. The functional based on the field **D** correctly reproduces this free energy, even though the functional was originally proposed as a minimum principle.

When used in molecular dynamics codes, it is important to choose functionals which are not too stiff. We emphasized that the ratio of the largest to smallest eigenvalue in the quadratic form is closely related to the number of time steps which are required to sample all modes. Again the functional based on the vector field **D** seems to display good scaling.

We used a model of a virus to implement and compare the optimization of four free energy functionals. The Legendre-transformed functional shows faster convergence and a greater accuracy in our tests. We suspect that this is linked to the lower stiffness of the Legendre formulation of the free energy.

■ APPENDIX I: SPHERICAL SYMMETRY AND DISCRETIZATION

Our study of determinant identities brought out the importance of discretizations that conserve the adjoint relation between the divergence and gradient operators. Such identities are also important for our study of the minimization of the polyelectrolyte free energy. Non-compatible discretizations give rise to numerical errors which are different between the different formulations. We now show how to discretize within a spherical geometry in such a way as to include important dualities between the discretized equations. The potentials ϕ and Ψ are defined on the points of the discretization, while $\nabla\phi$, $\nabla\Psi$, and **D** are defined on intermediate links. We wish to conserve the fundamental identity

$$\int \mathbf{D}\cdot\nabla\phi = -\int \phi \operatorname{div} \mathbf{D} + \oint \phi\mathbf{D} \, \mathrm{d}S \tag{51}$$

The discretized left-hand side of this equation gives

$$4\pi \sum_n r_{n,n+1}^2 \left(\frac{\phi_{n+1} - \phi_n}{\delta}\right)\mathbf{D}_{n,n+1} \tag{52}$$

where we have used the simplest differencing scheme for the gradient operator, and we define $r_{n,n+1}$ as the position of the center of the link. Identifying both sides of the identity, a definition of the discretized divergence is obtained:

$$\operatorname{div}_n \mathbf{D} = \frac{\mathbf{D}_{n,n+1}r_{n,n+1}^2 - \mathbf{D}_{n-1,n}r_{n-1,n}^2}{\delta r_n^2} \tag{53}$$

The Laplacian operator is then defined as usual by $\nabla^2 = -\operatorname{div}_n \operatorname{grad}$.

■ APPENDIX II: ONE-LOOP FREE ENERGIES

We give here the treatment of the one-loop correction in a homogeneous electrolyte. The free energy (compared with the free energy of an empty box) coming from quadratic fluctuations is

$$F_f = \frac{k_BT}{2} \sum_q \log\left(1 + \frac{\kappa^2}{q^2}\right) \tag{54}$$

$$= \frac{k_BT}{(2\pi)^2} \int_0^{q_0} q^2 \, \mathrm{d}q \, \log(1 + \kappa^2/q^2) \tag{55}$$

$$= \frac{k_BT}{(2\pi)^2}\left(\kappa^2 q_0 - \frac{\pi\kappa^3}{3}\right) + O(1/q_0) \tag{56}$$

where we introduce an upper cut-off q_0. The divergence in q_0[1] can be balanced by a purely local self-energy of the form $1/(2q^2)$ corresponding to the Born energy $1/8\pi\varepsilon a$ per atom, with a being a real-space cutoff. The long-ranged Debye–Hückel energy to the electrolyte is then

$$\frac{F_{DH}}{V} = -\frac{k_BT\kappa^3}{12\pi} \tag{57}$$

which comes from

$$F_{DH} = \frac{k_BT}{2} \sum_q \left(\log(1 + \kappa^2/q^2) - \lambda\beta e^2/(\varepsilon q^2)\right) \tag{58}$$

■ AUTHOR INFORMATION

Corresponding Authors
*E-mail: justine.pujos@espci.org.
*E-mail: anthony.maggs@espci.fr.

Notes
The authors declare no competing financial interest.

■ REFERENCES

(1) Allen, R.; Hansen, J.-P.; Melchionna, S. *Phys. Chem. Chem. Phys.* **2001**, *3*, 4177–4186.
(2) Fogolari, F.; Briggs, J. M. *Chem. Phys. Lett.* **1997**, *281*, 135–139.
(3) Reiner, E. S.; Radke, C. J. *J. Chem. Soc., Faraday Trans.* **1990**, *86*, 3901–3912.
(4) Stengel, M.; Spaldin, N. A.; Vanderbilt, D. *Nat. Phys.* **2009**, *5*, 304–308.
(5) Landau, L.; Lifshits, E.; Lifshits, E.; Pitaevskiĭ, L. *Electrodynamics of continuous media: Pergamon international library of science, technology, engineering, and social studies*; Pergamon: Oxford, 1984.
(6) Kirzhnits, D. A. *Sov. Phys.-Usp.* **1987**, *30*, 575.
(7) Dolgov, O.; Kirzhnits, D.; Maksimov, E. *Rev. Mod. Phys.* **1981**, *53*, 81–93.
(8) Maggs, A. C. *EPL* **2012**, *98*, 16012.
(9) Pujos, J. S.; Maggs, A. C. Legendre transforms for electrostatic energies. 2012. http://arxiv.org/abs/1211.6601, cite arxiv:1211.6601 Comment: 7 pages. CECAM workshop: New Challenges in Electrostatics of Soft and Disordered Matter (May 7–10, 2012). http://www.cecam.org/workshop-0-689.html.
(10) Arnold, A.; Breitsprecher, K.; Fahrenberger, F.; Kesselheim, S.; Lenz, O.; Holm, C. *Entropy* **2013**, *15*, 4569–4588.
(11) Car, R.; Parrinello, M. *Phys. Rev. Lett.* **1985**, *55*, 2471–2474.
(12) Rottler, J.; Maggs, A. C. *Phys. Rev. Lett.* **2004**, *93*, 170201.
(13) Jadhao, V.; Solis, F. J.; de la Cruz, M. O. *Phys. Rev. E* **2013**, *88*, 022305.
(14) Solis, F.; Jadhao, V.; Olvera de la Cruz, M. *Phys. Rev. E* **2013**, *88*, 053306.
(15) Jadhao, V.; Solis, F.; de la Cruz, M. *Phys. Rev. Lett.* **2012**, *109*, 223905.
(16) Maggs, A. C. *J. Chem. Phys.* **2004**, *120*, 3108–3118.
(17) Maggs, A. C. *J. Chem. Phys.* **2002**, *117*, 1975–1981.

(18) Pasquali, S.; Maggs, A. C. *J. Chem. Phys.* **2008**, *129*, -.
(19) Podgornik, R.; Zeks, B. *J. Chem. Soc., Faraday Trans. 2* **1988**, *84*, 611−631.
(20) Netz, R. R.; Orland, H. *EPL* **1999**, *45*, 726.
(21) Wang, Z.-G. *Phys. Rev. E* **2010**, *81*, 021501.
(22) Zia, R. K. P.; Redish, E. F.; McKay, S. R. *Am. J. Phys.* **2009**, *77*, 614−622.
(23) Buyukdagli, S.; Achim, C. V.; Ala-Nissila, T. *J. Chem. Phys.* **2012**, *137*, 104902.
(24) Buyukdagli, S.; Ala-Nissila, T. *J. Chem. Phys.* **2014**, *140*, 064701.
(25) Naji, A.; Kanduč, M.; Forsman, J.; Podgornik, R. *J. Chem. Phys.* **2013**, *139*, 150901.
(26) Xu, Z.; Maggs, A. *J. Comput. Phys.* **2014**, *275*, 310−322.
(27) Koehl, P.; Delarue, M. *J. Chem. Phys.* **2010**, *132*, 064101.
(28) Lu, B.; Zhou, Y.; Holst, M.; McCammon, J. *Commun. Comput. Phys.* **2008**, *3*, 973−1009.
(29) Edwards, S. F. *Proceedings of the Physical Society* **1965**, *85*, 613.
(30) de Gennes, P.-G. *Scaling Concepts in Polymer Physics*; Cornell University Press, 1979; Chapter IX.2. Self-Consistent Fields.
(31) Šiber, A.; Podgornik, R. *Phys. Rev. E* **2008**, *78*, 051915.
(32) Siber, A.; Bozic, A. L.; Podgornik, R. *Phys. Chem. Chem. Phys.* **2012**, *14*, 3746−3765.
(33) Borukhov, I.; Andelman, D.; Orland, H. *J. Phys. Chem. B* **1999**, *103*, 5042−5057.
(34) Dennis, J. E., Jr.; More, J. J. *SIAM Rev.* **1977**, *19*, 46−89.
(35) Sorensen, D. C. *SIAM J. Numerical Anal.* **1982**, *19*, 409−426.